J. Fluid Mech. (2024), *vol*. 988, A9, doi:10.1017/jfm.2024.437

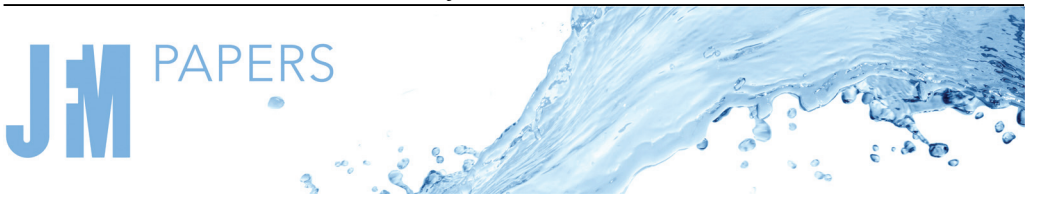

Sedimentation dynamics of passive particles in dilute bacterial suspensions: emergence of bioconvection

Bryan O. Torres Maldonado[1], Shravan Pradeep[1,2], Ranjiangshang Ran[1], Douglas Jerolmack[1,2] and Paulo E. Arratia[1,†]

[1]Department of Mechanical Engineering and Applied Mechanics, University of Pennsylvania, Philadelphia, PA 19104, USA

[2]Department of Earth and Environmental Science, University of Pennsylvania, Philadelphia, PA 19104, USA

(Received 15 December 2023; revised 22 March 2024; accepted 21 April 2024)

Microorganisms are ubiquitous in nature and technology. They inhabit diverse environments, ranging from small river tributaries and lakes, to oceans, as well as wastewater treatment plants and food manufacturing. In many of these environments, microorganisms coexist with settling particles. Here, we investigate the effects of microbial activity (swimming *E. coli*) on the settling dynamics of passive colloidal particles using particle tracking methods. Our results reveal the existence of two distinct regimes in the correlation length scale (L_u) and the effective diffusivity of the colloidal particles (D_{eff}), with increasing bacterial concentration (ϕ_b). At low ϕ_b, the parameters L_u and D_{eff} increase monotonically with increasing ϕ_b. Beyond critical ϕ_b, a second regime is found where both D_{eff} and L_u are independent of ϕ_b. We demonstrate that the transition between these regimes is characterized by the emergence of bioconvection. We use experimentally measured particle-scale quantities L_u and D_{eff} to predict the critical bacterial concentration for the diffusion–bioconvection transition.

Key words: bioconvection, swimming/flying, active matter

1. Introduction

Microorganisms are ubiquitous in both natural environments and technological applications. They are highly adaptable and inhabit diverse ecosystems such as swamps, oceans and rivers (Schallenberg & Kalff 1993; Nealson 1997; Herndl & Reinthaler 2013; Roberto, Van Gray & Leff 2018; Zhang *et al.* 2020). They also play a significant role

† Email address for correspondence: parratia@seas.upenn.edu

in numerous engineering applications (Falkowski, Barber & Smetacek 1998; Savage 2011; Falkowski 2012), including fermentation processes for vaccine and food production, and wastewater treatment processes (Swartz 2001; van Loosdrecht & Brdjanovic 2014; Lorenzo *et al.* 2018; Honda *et al.* 2023). Controlling the sedimentation process in biofuel production, for instance, can lead to improvements in algae separation from the fluid medium and an accumulation of algal biomass at the bottom of the production pond (Savage 2011).

Suspensions of swimming microorganisms (e.g. *E. coli*) or active particles (e.g. phoretic colloids) are typical examples of so-called active fluids (Ramaswamy 2010; Marchetti *et al.* 2013; Patteson, Gopinath & Arratia 2016*a*; Moran & Posner 2017). In these fluids, the constituents inject energy, generate mechanical stresses, and create flows within the fluid medium. Thus active fluids are systems that are inherently out of equilibrium even in the absence of external forces (Dabelow, Bo & Eichhorn 2019). Bacterial activity can lead to many complex phenomena such as reduced shear viscosity (Rafaï, Jibuti & Peyla 2010; Gachelin *et al.* 2013; López *et al.* 2015), hindrance in mixing and transport of passive scalars (Ran *et al.* 2021), formation of biofilms (Pradeep & Arratia 2022), and diffusion enhancement (Kim & Breuer 2004; Leptos *et al.* 2009; Thiffeault & Childress 2010; Kurtuldu *et al.* 2011; Miño *et al.* 2011; Jepson *et al.* 2013). In the dilute regime, particle (or tracer) diffusivity has been shown to increase linearly with bacteria concentration (Wu & Libchaber 2000), but depends on microorganism swimming behaviour (Chen *et al.* 2007) and particle size (Patteson *et al.* 2016*b*). Recent work has shown that the enhanced diffusion dynamics in the presence of bacteria can lead to large-scale clustering of particles (Bouvard, Moisy & Auradou 2023). However, less understood are the effects of bacterial activity on the settling dynamics of tracer particles.

Initial studies have largely focused on steady-state analysis (Palacci *et al.* 2010; Maggi *et al.* 2013; Ginot *et al.* 2015). These include sedimentation studies with active Janus particles that show (steady-state) density profiles that decay exponentially with system height (Palacci *et al.* 2010; Ginot *et al.* 2015, 2018). The resulting length scale is larger than expected for thermal equilibrium systems, which is explained through the introduction of an effective temperature (and diffusivity) with values that far exceed those of passive systems (Palacci *et al.* 2010). These findings are corroborated by theory and simulations with no (or limited) hydrodynamic interactions (Tailleur & Cates 2008; Nash *et al.* 2010; Wang *et al.* 2014; Ginot *et al.* 2018; Vachier & Mazza 2019). Experiments with swimming *E. coli* show that bacteria aggregation (due to extra-cellular polymer) can have significantly enhanced sedimentation rates (Maggi *et al.* 2013), while particles settling in suspensions of *C. reinhardtii* show the familiar exponential concentration profile but with an effective gravitational length (or diffusivity) that is proportional to algae concentration (Jeanneret *et al.* 2016). These studies show that the concept of effective diffusivity (and temperature) can be useful in characterizing the steady sedimentation profiles of active suspensions.

Only recently have time-dependent sedimentation (that is, concentration) profiles of bacterial suspensions been investigated; see Singh *et al.* (2021) and Torres Maldonado *et al.* (2022). These studies show that in the dilute regime, bacteria activity can significantly hinder the sedimentation process (Singh *et al.* 2021). At vanishingly low bacteria concentration (ϕ_b), the (time-dependent) concentration profiles can be accurately described by an advection–diffusion equation; however, as ϕ_b is increased, sink–source terms must be introduced in the formulation to account for bacteria population dynamics, including a dispersivity parameter that increases with ϕ_b (Singh *et al.* 2021). In this regime, the bacterial suspension undergoes phase separation, and bacteria settling speed is found to be strongly correlated with a time scale associated with oxygen depletion

within the system (Torres Maldonado *et al.* 2022). These studies highlight the role of oxygen in the sedimentation of living suspensions; microorganisms are known to exhibit aerotaxis, a phenomenon that prompts aerobic bacteria to seek an oxygen source (Wager 1911; Baracchini & Sherris 1959; Adler *et al.* 2012; Bouvard *et al.* 2022). When suspended in a relatively deep layer of fluid, the microorganism can deplete the oxygen concentration in the water while oxygen continuously diffuses in from the air–water interface above. In response, microorganisms swim towards the oxygen concentration gradient and generate fluid motion, a phenomenon referred to as bioconvection driven by aerotaxis (Hillesdon, Pedley & Kessler 1995; Jánosi, Kessler & Horváth 1998). During bioconvection, oxygen-enriched water descends from the interface, giving rise to a complex convection-dependent gradient that guides the swimming bacteria. Analysis predicts that the emergence of bioconvection occurs beyond a critical Rayleigh number (Hillesdon & Pedley 1996), a dimensionless number that quantifies the ratio of the buoyancy forces to viscous forces (Hill, Pedley & Kessler 1989), although bioconvection can also occur from phototaxis and thus be controlled by a light source (Arrieta *et al.* 2019). While extensive research has focused on elucidating the mechanisms behind bioconvection formation (Pedley & Kessler 1992; Hill & Pedley 2005; Bees 2020), limited experimental work has been conducted to corroborate these theoretical predictions.

In this contribution, we experimentally investigate the sedimentation dynamics of colloidal particles and the formation of bioconvection patterns in dilute bacterial suspensions using particle tracking methods. We find that bacterial activity has a significant impact on particle diffusivity, leading to the identification of two dynamical regimes. Initially, as bacterial concentration is increased, we observed a corresponding linear increase in diffusivity. However, as bacterial concentration is further increased (but still dilute), particle diffusivity becomes independent of bacterial concentration. This transition coincides with the inception of bioconvection patterns above a critical Rayleigh number (Γ_{cr}) (Hillesdon & Pedley 1996).

2. Materials and methods

We experimentally investigate the sedimentation dynamics of spherical colloids in the presence of bacterial activity. Active fluids are mixtures of bacterial suspensions and passive particles suspended in deionized water to reach the desired volume fractions of bacteria and particles, denoted as ϕ_b and ϕ_p. Bacterial suspensions are prepared using wild-type *Escherichia coli* (K12 MG1655), which are cultured to saturation (10^9 cells ml^{-1}) in LB broth (Sigma-Aldrich). Passive particles are polystyrene spheres (density $\rho_p = 1.05$ g cm^{-3}, Thermo Scientific) with diameter $d = 3.2$ μm, which are gently cleaned by centrifugation (Centrifuge 5430, Eppendorf). All active suspensions are contained within a custom-made quasi-two-dimensional sedimentation cell constructed from optically transparent polymethyl methacrylate (PMMA) material, offering optimal clarity (see figure 1*a*). The container measures 100 mm in height, 28 mm in width, and 400 μm in thickness, and is assembled using precision laser cutting and chemical bonding techniques (Sun *et al.* 2007).

Active fluids are homogenized manually using a pipette before being introduced into the custom-made PMMA container. A volume ≈1.1 ml of the prepared fluid is then transferred into the container, as depicted schematically in figure 1(*a*). Subsequently, the container is immersed in a water tank to maintain the fluid at room temperature 24 °C. Images are captured at frame rate 30 fps with a high-resolution camera (IO Industries, Flare 4M180) and a microscope (Infinity, K2) equipped with a 10× objective. The light

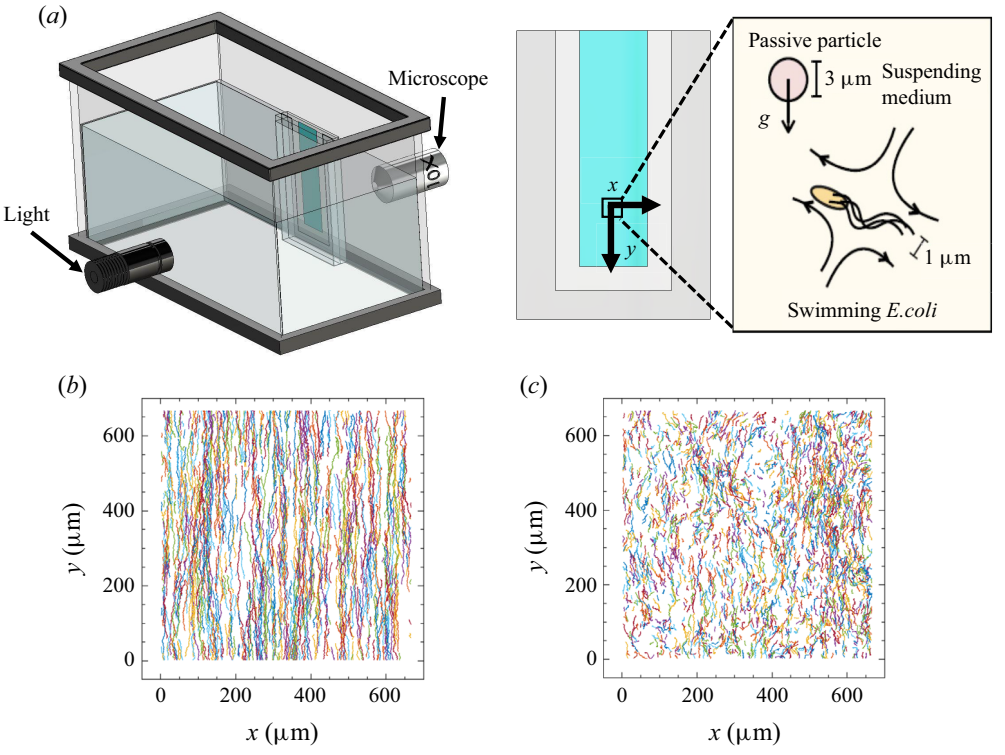

Figure 1. Experimental set-up and sample particle trajectories. (*a*) A schematic of the set-up and bacteria/particle suspensions (active fluid). Sedimentation experiments are conducted in an optically clear rectangular container. The particles are 3.2 μm polystyrene spheres, and the bacteria are 2 μm rod-shaped *E. coli*; both are subjected to gravity. Particles located at the centre and at a height ≈20 mm from the bottom of the container are observed through a microscope. These spherical colloidal particles are tracked through a particle tracking velocimetry method. Particle trajectories ($\phi_p = 0.04\,\%$) tracked for total time 10 minutes are shown in (*b*) without bacteria and in (*c*) with bacteria ($\phi_b = 0.45\,\%$). When particles and *E. coli* are combined, the passive particle trajectories in the lateral direction undergo significant modifications compared to their trajectories in the absence of bacteria.

source used is a single-colour cold visible LED (M490L4, Thor Labs). The depth of field of the microscope is 3.5 μm. All the measurements are taken at height 20 mm from the base of the sedimentation cell. Additionally, we focus at the half-distance, at ∼200 μm from either side of the walls, to avoid the cell wall effects on the hydrodynamic hindrance of fluctuations from the bacterial activity on our passive colloidal particles. Later in the paper we show that under these experimental conditions, we are able to match the Stokes–Einstein diffusion coefficient and the corresponding settling velocity of a single particle to that of passive colloids in the absence of bacterial activity. This confirms that our experimental conditions are devoid of wall effects.

The initial volume fraction ϕ_b of motile bacteria in the container varies from 0 % (0 cells ml^{-1}) to 0.75 % (5.4×10^9 cells ml^{-1}), while the volume fraction of spherical colloids is maintained consistently at $\phi_p = 0.04\,\%$. It is worth noting that both ϕ_b and ϕ_p concentrations are within the dilute regime ($\phi < 1\,\%$), and no significant macroscopic collective behaviour is observed in these bacteria–particle suspensions under the microscope (Patteson *et al.* 2016*b*; Singh *et al.* 2021). The selected range of ϕ_b in this study remains below the threshold at which collective motion is typically observed

($\approx 10^{10}$ cells ml^{-1}) (Kasyap, Koch & Wu 2014). All captured images for the suspensions are acquired within a 30 minute time frame. Importantly, within this designated time frame, no noteworthy reduction in bacteria motility is observed, a finding that has been corroborated by recent investigations (Ran *et al.* 2021; Singh *et al.* 2021).

3. Results and discussion

The main goal is to understand the interplay between bacterial activity and the settling dynamics of passive spherical particles. To this end, we use particle tracking techniques to visualize the colloidal particle's Lagrangian trajectories (Crocker & Grier 1996). Sample particle trajectories from passive ($\phi_p = 0.04\,\%$, no bacteria) and active ($\phi_p = 0.04\,\%$, $\phi_b = 0.45\,\%$) fluids are shown in figures 1(*b*) and 1(*c*), respectively. The passive fluid case shows particle trajectories predominately in the downward direction ($-y$) with apparent noise along the x-axis. For the active fluid, on the other hand, particle paths show amplified displacement along the x-axis, indicating that bacterial activity induces modifications to the colloidal particle downward trajectories. This trajectory enhancement (in the x-axis) manifests itself consistently across all experiments, providing an explanation for the previously observed hindrance in the speed of the particle front (Singh *et al.* 2021; Torres Maldonado *et al.* 2022). These qualitative findings show that bacteria modify the settling trajectories of colloidal particles through hydrodynamic interactions, even in the dilute regime ($\phi_b < 1\,\%$).

3.1. *Characterizing length scales of particle correlations*

We quantify the sedimentation dynamics of our fluid by computing its time-dependent velocity fields using an in-house particle imaging velocimetry method (Li *et al.* 2021; Brosseau *et al.* 2022; Ran *et al.* 2022). The goal is to understand how bacterial activity (ϕ_b) alters the spatial correlation functions of particle fluctuations (Segrè, Herbolzheimer & Chaikin 1997; Tee *et al.* 2002). Here, the spatial correlation function of the velocity fluctuations, $C_u(r_x)$, is defined as

$$C_u(r_x) = \langle u(x)\, u(x + r_x)\rangle / \langle u^2\rangle, \tag{3.1}$$

where x represents the direction perpendicular to gravity, $\langle\cdot\rangle$ denotes an ensemble average across all spherical particles, $u(x)$ denotes the local velocity of a particle at position x', and r_x denotes distance in the direction parallel to the sedimentation. Notably, $u(x)$ incorporates contributions from both particle self-diffusivity and hydrodynamic interactions. In the absence of bacteria ($\phi_b = 0\,\%$), we observe a decay in the spatial correlation length scales at small distances (figure 2*a*). With an increase in ϕ_b, we identify a corresponding increase in spatial correlation functions over larger distances. However, as $\phi_b \geq 0.45\,\%$, the spatial correlation functions become independent of ϕ_b. To analyse this trend quantitatively, we calculate the integral length scale of velocity L_u as shown in figure 2(*b*). This integral length scale is defined as $L_u = \int_0^\infty C_u(r_x)\,\mathrm{d}r_x$. Results shows that L_u increases linearly as ϕ_b is increased (figure 2*b*), but this relationship weakens and L_u becomes independent of ϕ_b for $\phi_b \geq 0.45\,\%$. These findings show a positive correlation between L_u and ϕ_b up to $\phi_b \geq 0.45\,\%$. This outcome aligns with previous research, highlighting the presence of two distinct regimes within the sedimentation process (Torres Maldonado *et al.* 2022).

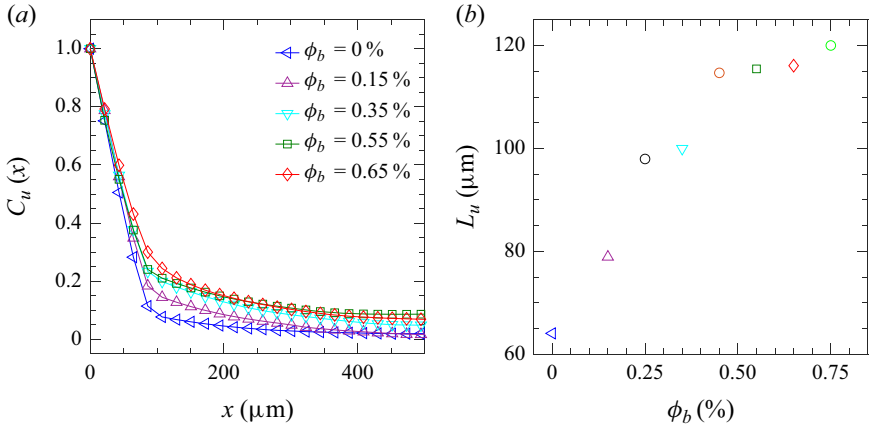

Figure 2. (*a*) The spatial correlation functions of particle velocities (u) in the lateral direction across the x-axis. (*b*) The integral length scale of the lateral velocities at different bacteria volume fractions ϕ_b. The open circular symbols from left to right represent the results at $\phi_b = 0.25\,\%$ (black), $\phi_b = 0.45\,\%$ (orange) and $\phi_b = 0.75\,\%$ (light green). The presence of bacteria leads to an increase in correlation functions, and subsequently to an increase in length scales.

3.2. *Mean square displacements and diffusivity*

Next, we use experimentally measured particle tracks to compute the mean square displacements of the passive particles as a function of ϕ_b. The mean square displacement is defined as $MSD(\Delta t) = \langle |\boldsymbol{r}(t_R + \Delta t) - \boldsymbol{r}(t_R)|^2 \rangle$, where t_R is denoted as the reference time. First, we extract the distance vector $\boldsymbol{r}$ in the direction perpendicular to gravity, r_x, yielding the mean square displacement along the x-axis (MSD_x). As shown in figure 3(*a*), MSD_x exhibits diffusive behaviour (at sufficiently long time intervals) that increases with ϕ_b. We can estimate an effective diffusivity D_{eff} by fitting $MSD_x = 2D_{eff}\,\Delta t$ to the experimental data at long times, and find that, similar to L_u, D_{eff} grows linearly with ϕ_b followed by an asymptote for $\phi_b \geq 0.45\,\%$ (figure 3*c*). Similarly, we compute the mean square displacements of the tracked particles relative to the y-axis ($MSD_{y'}$) as a function of ϕ_b. Notably, we subtract the mean sedimentation rates along the y-axis since our focus is on understanding how bacteria activity affects particle fluctuations, i.e. $y' = y - \langle y \rangle$. Figure 3(*b*) shows that $MSD_{y'}$ exhibits diffusive behaviour that increases with increasing ϕ_b. We apply a similar fitting approach, relating $MSD_{y'}$ to D_{eff} as shown in figure 3(*c*) (filled symbols). Our results reveal that for the control case ($\phi_b = 0\,\%$), $D_{eff} = 0.150 \pm 0.001\ \mu\text{m}^2\ \text{s}^{-1}$ for MSD_x, and $D_{eff} = 0.145 \pm 0.001\ \mu\text{m}^2\ \text{s}^{-1}$ for $MSD_{y'}$. These measurements align with the theoretically predicted value from the Stokes–Einstein relation, $D_0 = k_B T/(3\pi\mu d) = 0.150\ \mu\text{m}^2\ \text{s}^{-1}$ (Einstein 1905), where k_B represents the Boltzmann constant, μ is the fluid viscosity, and T denotes the temperature. These results indicate that hydrodynamic interactions among passive particles in our study are relatively weak, which is not surprising given the dilute particle volume fraction ($\phi_p = 0.04\,\%$).

Overall, the mean square displacement measurements of particles in the presence of motile bacteria exhibit an increasing trend as ϕ_b rises, as shown in figures 3(*a*) and 3(*b*). This enhancement on particle displacement leads to a corresponding increase in D_{eff}, illustrated in figure 3(*c*). By comparison, a similar experiment was conducted using non-motile bacteria ($\phi_{d,b} = 0.35\,\%$), as shown in figures 3(*a*) and 3(*b*). Here, we observe a negligible increase in mean square displacement compared to the absence of

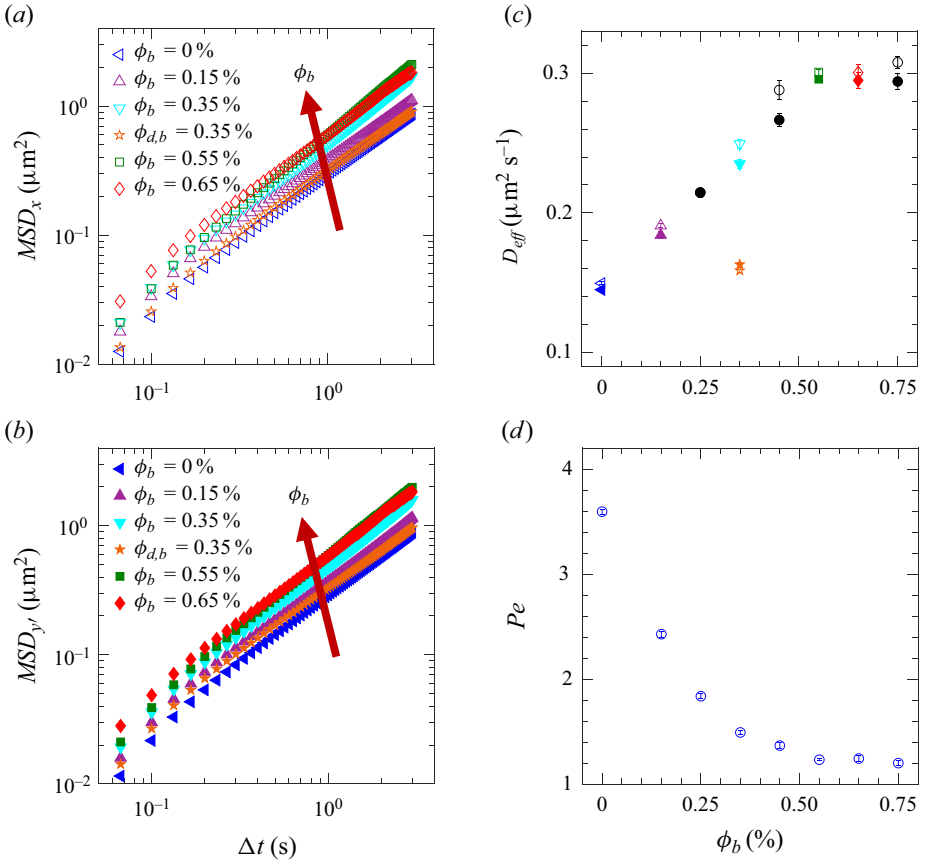

Figure 3. (*a*) Mean square displacement in the *x*-axis (MSD_x) of spherical particles at different bacteria volume fractions ϕ_b. (*b*) Mean square displacement of particle fluctuations in the *y*-axis ($MSD_{y'}$) at different ϕ_b. (*c*) Effective particle diffusivities D_{eff} from MSD_x (open symbols) and MSD_y (closed symbols) as functions of ϕ_b. The presence of swimming *E. coli* increases particle fluctuations in both the *x* and *y* directions, resulting in higher D_{eff}. (*d*) Péclet number (Pe) as a function of ϕ_b. The results demonstrate that the presence of bacteria enhances diffusion transport in the settling process, eventually reaching a plateau regime where advection and diffusion transport are in close balance ($Pe \approx 1$).

bacteria ($\phi_b = 0\,\%$), resulting in $D_{eff} = 0.159 \pm 0.001$ μm^2 s^{-1} along the *x*-axis and $D_{eff} = 0.163 \pm 0.002$ μm^2 s^{-1} along the *y*-axis for $\phi_{d,b} = 0.35\,\%$ (figure 3*c*). These results indicate that the presence of non-motile bacteria exerts negligible impact on particle diffusivity and hydrodynamic interactions. This small but finite effect is likely due to residual motility after bacteria is exposed to ultraviolet (UV) light; that is, there is a small bacterial population that is still motile after the UV treatment. In other words, the observed enhancement in particle diffusivity across the experiments with bacteria is primarily attributed to bacterial activity within the suspension; as mentioned before, D_{eff} exhibits a nearly linear relationship with bacteria concentration up to $\phi_b \leq 0.45\,\%$. Surprisingly, however, D_{eff} (and L_u) become independent of ϕ_b for $\phi_b \geq 0.45\,\%$; see figures 2(*b*) and 3(*c*). The macroscopic signature of this behaviour can be captured by computing the Péclet number, defined as $Pe = V_p d/(2\langle D_{eff}\rangle)$. Here, V_p is the average settling speed of particles, which has been measured previously for the same fluids and conditions (Torres Maldonado *et al.* 2022). We note that the sedimentation speed for our

control case, V_p, is $0.33 \pm 0.0006\ \mu\text{m s}^{-1}$. In comparison, the associated velocity, known as the Stokes settling speed, is given as $V_0 = 2a^2\,\Delta\rho\, g/9\eta$, where a is the particle radius, $\Delta\rho$ is the density difference between the particle and the solvent, g is the acceleration due to gravity, and η is the solvent viscosity, which for 3.2 μm particle diameter is $0.33\ \mu\text{m s}^{-1}$ (Russel *et al.* 1991). A small *Pe* signifies the dominance of diffusion in particle transport, while a large *Pe* indicates the prevalence of advection. Figure 3(*d*), shows that *Pe* decreases as ϕ_b increases, but it reaches a plateau at $Pe \approx 1$, indicating a point at which advection and diffusion transport are in close balance.

This asymptotic behaviour has also been observed in macroscopic quantities such as the hindering settling function $H(\phi)$ for the same type of active fluids and in similar range of ϕ_b (Torres Maldonado *et al.* 2022). These results show a different trend compared to prior studies of (passive) particles in active suspensions, where gravity and oxygen gradients do not play a role, and bioconvection is not observed. They demonstrate that D_{eff} increases linearly with ϕ_b up to $\phi_b \approx 1\,\%$ (Wu & Libchaber 2000; Leptos *et al.* 2009; Patteson *et al.* 2016*b*). A possible explanation is that motile bacteria likely undergo a transition in their swimming motion, shifting from a random pattern to 'organized' trajectories, within the range $\phi_b \geq 0.45\,\%$ (still dilute). One possibility is the development of bioconvection patterns (Hill *et al.* 1989; Hillesdon & Pedley 1996). We will explore this possibility below.

3.3. *Unveiling the phenomenon of bioconvection*

Our study involves a suspension containing *E. coli*, which is known for its oxygen-seeking behaviour, termed aerotaxis. Following previous work (Hillesdon & Pedley 1996), we define a dimensionless parameter Γ that is analogous to the Rayleigh number in thermal convection problems:

$$\Gamma = \frac{(\rho_b - \rho_w)\phi_b g L_u^3}{\rho_w \nu D_{eff}}, \tag{3.2}$$

where $\rho_b = 1.105\ \text{g cm}^{-3}$ (Martínez-Salas, Martín & Vicente 1981) and $\rho_w = 1.0\text{g cm}^{-3}$ represent the densities of bacteria and water, respectively, g is the acceleration due to gravity, and ν denotes the kinematic viscosity of water. The only difference between our formulation and prior work is the length scale that we employ (Hillesdon & Pedley 1996). Our present approach incorporates a length scale associated with the particle dynamics (i.e. L_u), which is directly measured from the spatial correlation functions. Figure 4(*a*) shows that Γ increases linearly with ϕ_b, as expected.

Next, following a linear stability analysis, one can define a critical Rayleigh-like number (Γ_{cr}) that describes the relative importance of bacterial diffusion to bioconvection (aerotactic behaviour plus density difference) behaviour (Hillesdon & Pedley 1996). Initially, it is necessary to establish two dimensionless constants stemming from the equations governing cell and oxygen conservation. The first of these constants, denoted as β, characterizes the relationship between the rate of oxygen consumption and the rate of oxygen diffusion. It is defined as

$$\beta = \frac{K_0 n_0 L_u^2}{D_c C_0}, \tag{3.3}$$

where K_0 is the oxygen consumption rate, n_0 is the initial cell concentration, D_c represents oxygen diffusivity, and C_0 denotes the initial oxygen concentration. Here, we assume $K_0 \approx 2 \times 10^{-18}$ mol min^{-1} cell^{-1} (Schwarz-Linek *et al.* 2016), $D_c \approx 200\ \mu\text{m}^2\ \text{s}^{-1}$ (Han & Bartels 1996) and $C_0 \approx 0.0058$ ml O_2/ml H_2O (Carpenter 1966).

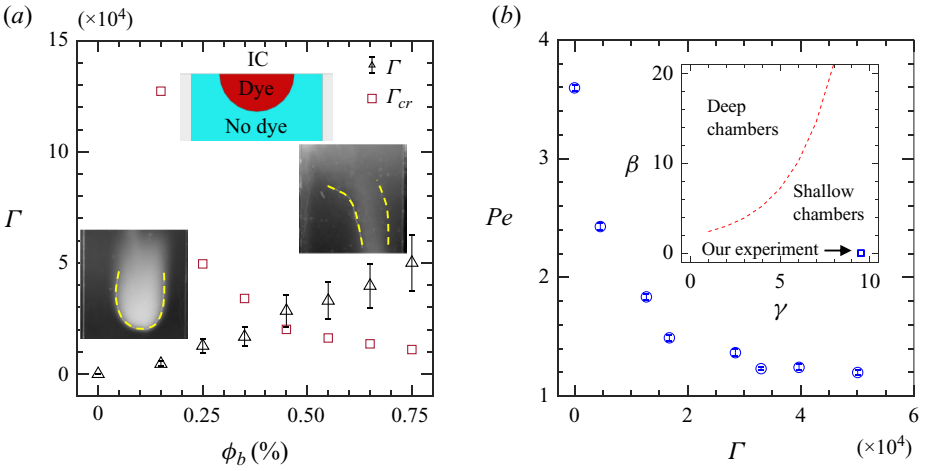

Figure 4. (*a*) Experimental Rayleigh number (Γ), and theoretical critical Rayleigh number (Γ_{cr}) as functions of bacteria volume fraction (ϕ_b). Results show a crossover of Γ across $\phi_b \approx 0.45\,\%$. When $\Gamma < \Gamma_{cr}$, swimming bacteria are not significantly affected by the oxygen at the top of the container. However, when $\Gamma > \Gamma_{cr}$, oxygen plays a significant role in the swimming behaviour of *E. coli*, leading to bioconvection. This explains the emergence of the plateau regime observed in settling experiments when $\phi_b \geq 0.45\,\%$. The inset at the top shows a schematic of the initial condition (IC) of the dye experiments, where red indicates the suspension with dye, and light blue represents the same suspension without dye. The inset on the left shows an illustrative snapshot of a dye experiment where $\phi_b < 0.45\,\%$, and on the right where $\phi_b \geq 0.45\,\%$, displaying bioconvection patterns. (*b*) Péclet number (*Pe*) as a function of experimental Rayleigh number (Γ), which shows that convective transport of colloidal particles is reduced with increased bacterial-driven convection. The inset shows the validity of (3.5) by using the inequality $\gamma\beta \leq \xi \tan^{-1}\xi$.

The second dimensionless constant, γ, quantifies the strength of oxytactic swimming relative to random diffusive swimming. It is expressed as

$$\gamma = \frac{cV_{sb}}{D_b}, \tag{3.4}$$

where c is the chemotaxis constant, V_{sb} represents bacteria swimming speed, and D_b is the bacteria diffusivity. Here, we assume $c = V_{sb}\tau_r$, where $\tau_r = 0.95$ s stands for the mean run time of *E. coli* (Patteson *et al.* 2015). Additionally, we take $D_b \approx 10\ \mu\text{m}^2\ \text{s}^{-1}$ and $V_{sb} \approx 10\ \mu\text{m s}^{-1}$ (Ran *et al.* 2021).

Our experiment can be approached as a shallow chamber, since it satisfies the inequality $\gamma\beta \leq \xi \tan^{-1}\xi$, wherein ξ is defined as $\xi^2 = e^{\gamma} - 1$ (inset of figure 4*b*). Therefore, Γ_{cr}, following Hillesdon & Pedley (1996), can be expressed as

$$\Gamma_{cr} = \frac{576}{\gamma\beta}. \tag{3.5}$$

We proceed to compute the experimental values of Γ and Γ_{cr} as functions of ϕ_b, as shown in figure 4(*a*). The data illustrate an increase in Γ with rising ϕ_b, while Γ_{cr} decreases with higher ϕ_b. This aligns with the expectation that higher ϕ_b leads to accelerated oxygen consumption by *E. coli* within the fluid. Remarkably, an intersection between Γ and Γ_{cr} occurs at $\phi_b \approx 0.45\,\%$, signifying the onset of bioconvection when $\phi_b \geq 0.45\,\%$. This observation could elucidate the plateau observed in D_{eff} and L_u, and in the macroscopic hindering settling function ($H(\phi)$) seen in previous experiments (Torres Maldonado *et al.* 2022). Concurrently, with the increase in Γ, the Péclet number (*Pe*) reaches a plateau at

unity for $\phi_b \geq 0.45\,\%$, as shown in figure 4(*b*). This strongly suggests that the reduction in convective transport of colloidal particles (*Pe*) results from the increased convective motion driven by swimming bacteria.

To further illustrate the existence of bioconvection in settling active fluids, we perform dye mixing experiments for a range of ϕ_b. These experiments involved introducing 100 µl of dye ($2.5 \times 10^{-3} M$ fluorescein aqueous solution) into bacterial solutions at the upper portion of the rectangular chamber within the experimental set-up. Image capture occurred every 2 minutes over a 14 hour period using a Nikon D7100 camera equipped with a 105 mm Sigma lens. Illumination was achieved using black light (USHIO, F8T5/BLB), peaking at 368 nm in the UV range. Importantly, 90 % of the UV energy falls within the long-wave UVA-I range (340–400 nm), and it minimally affects suspension activity (Vermeulen *et al.* 2008; Ran *et al.* 2021). As expected, experiments without bacteria ($\phi_b = 0\,\%$) demonstrated settling of the dye dominated by diffusion and moving directly downwards, evident in figure 5(*a*). Similarly, $\phi_b = 0.35\,\%$ experiments, with $\Gamma < \Gamma_{cr}$, displayed no significant convection patterns (figure 5*b*). However, experiments at $\phi_b = 0.75\,\%$, where $\Gamma > \Gamma_{cr}$, exhibited pronounced convection patterns (figure 5*c*). In the early stages, the dye exhibited anticlockwise motion due to convection, transitioning to complex bioconvection patterns in the upward direction at later times.

We quantify the dynamics observed in these images by computing the image correlation with respect to the initial image ($t = 0$ min). Figure 6 shows the image correlation for the no-bacteria ($\phi_b = 0\,\%$), $\phi_b = 0.35\,\%$ and $\phi_b = 0.75\,\%$ cases as functions of time to quantify the dye spreading process in the sedimentation cell. For the no-bacteria case, this process can be described by the diffusion equation plus the effects of gravity (i.e. droplet buoyancy) since there is a small density difference between the dye and the fluid. The solution to this equation, $\partial C/\partial t = D\,\boldsymbol{\nabla} \cdot C + g\,\Delta\rho$, is obtained numerically and shown in figure 6 as an inset; here, C is dye concentration, D is dye diffusivity, g is gravity, and $\Delta\rho$ is the density difference between dye and fluid. The numerical simulation seems to capture the time-dependent decorrelation trend for the passive case relatively well. For $\phi_b = 0.35\,\%$, decorrelation rates are initially similar to the no-bacteria case but start to deviate and slow down at $\Delta t \approx 30$ minutes. That is, bacterial activity hinders the settling behaviour of dye particles as the suspension transitions from diffusive-dominated behaviour to one dominated by bacterial-activity-induced convection. Macroscopically, this behaviour manifests itself by decreasing the hindered settling function $H(\phi)$ (where $H(\phi) = V_p(\phi)/V_0$, $V_p(\phi)$ is the mean sedimentation speed of the particles in the presence of bacteria, and V_0 is the Stokes settling speed), as reported in our earlier work (Torres Maldonado *et al.* 2022). As ϕ_b is increased further ($\phi_b = 0.75\,\%$), however, the correlation data show two distinct parts. At short times, the correlation shows a significant delay due to bioconvection-induced motion of the dye particles perpendicular to the gravity. At longer time scales, image correlations mirror the samples, with diffusion-like behaviour emerging due to the dye particles following the downward draft in bioconvection rolls. These results show delicate interplay between bacterial activity, oxygen diffusion (i.e. aerotactic behaviour) and density differences. Our results clarify the existence of two regimes in settling dynamics parameters observed in our present study (L_u, D_p and *Pe*) and previous work ($H(\phi)$) (Torres Maldonado *et al.* 2022), indicating that active suspensions are purely diffusive at $\phi_b < 0.45\,\%$ and are characterized with complex bioconvection patterns for $\phi_b \geq 0.45\,\%$.

Our experimental findings demonstrate that the presence of bacteria leads to an increase in both particle correlation length scales (figure 2) and their effective diffusivity values

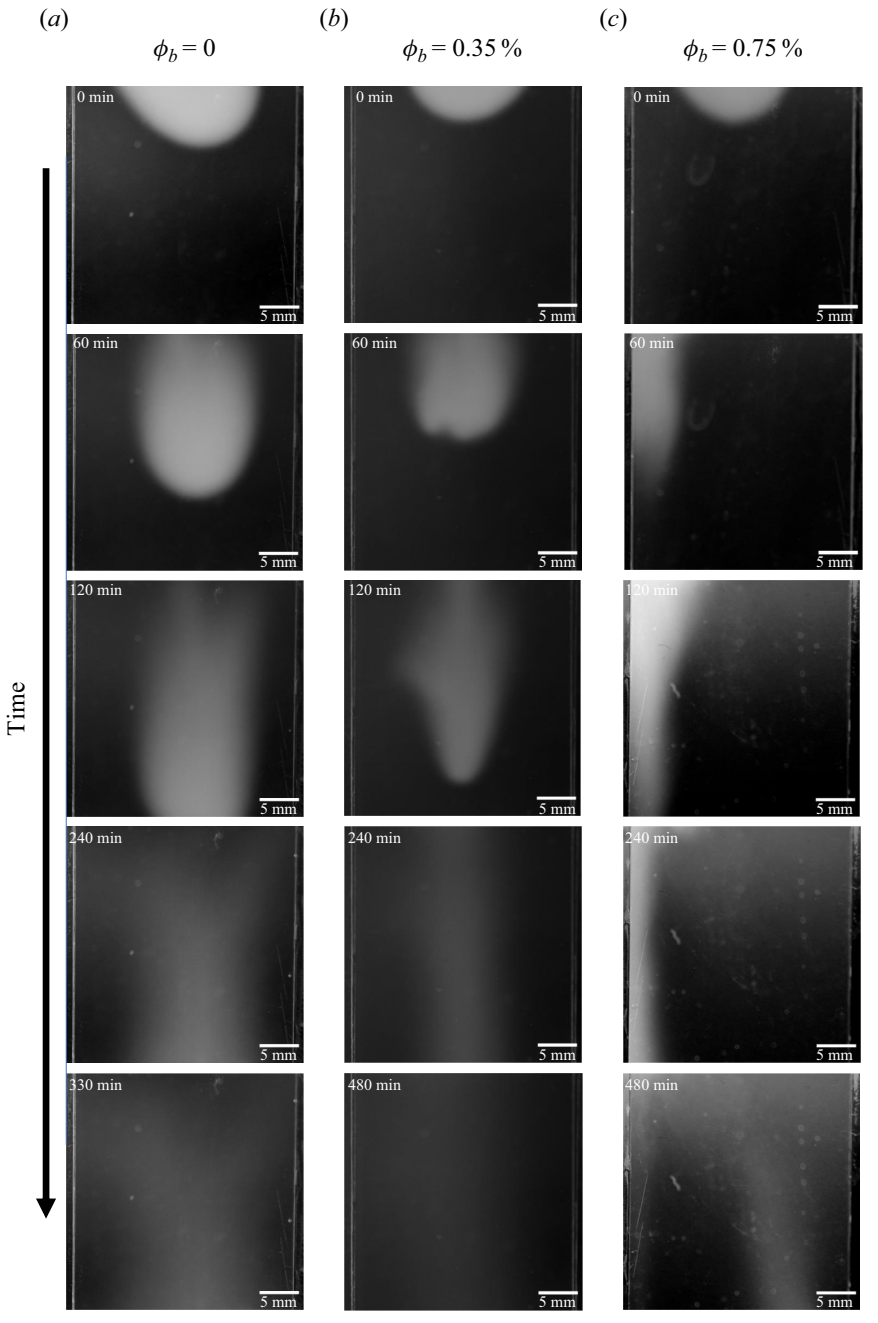

Figure 5. Representative snapshots of the time evolution of the settling suspensions with dye at the top of the settling container: (*a*) no bacteria ($\phi_b = 0\,\%$); (*b*) active bacteria at $\phi_b = 0.35\,\%$; (*c*) active bacteria at $\phi_b = 0.75\,\%$. Dye in passive suspensions shows that it settles straight downwards as a function of time. When bacteria are added, as shown in (*b*) ($\phi_b < 0.45\,\%$), the results show that dye settling is slightly hindered due to the random motion of bacteria. However, no significant bioconvection patterns were observed. When $\phi_b \geq 0.45\,\%$, as shown in (*c*), dye gets convected in an anticlockwise motion. Dye returns to the field of view from below at long times, showing that bioconvection is observed in this case.

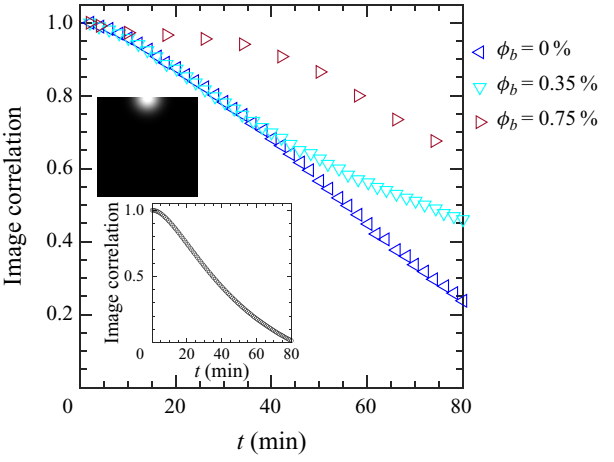

Figure 6. Temporal evolution of image correlation in dye experiments as a function of time, for no bacteria ($\phi_b = 0\,\%$), $\phi_b = 0.35\,\%$ and $\phi_b = 0.75\,\%$. For concentrations $\phi_b < 0.45\,\%$, the correlation is reminiscent of pure diffusive behaviour throughout the observation period. However, for $\phi_b > 0.45\,\%$, the image correlation showed a significant delay due to bacteria, which convects the dye perpendicular to the direction of gravity and subsequently exhibits diffusive behaviour. The top inset shows the numerical simulation of a point source with an initial condition similar to the image in the top left of figure 5, and the bottom inset shows the corresponding decorrelation with time; see text for details.

D_{eff} (figure 3). As mentioned before, these measurements exhibit a linear increase up to approximately $\phi_b \approx 0.45\,\%$. Beyond this threshold ($\phi_b \geq 0.45\,\%$), both L_u and D_{eff} remain constant, establishing their independence from ϕ_b. These experimental results align with our prior findings, wherein the hindered settling function $H(\phi)$ of the particle front showed a linear decrease with bacterial concentration for $\phi_b < 0.45\,\%$. The hindered settling function $H(\phi)$ of the particle front ultimately reaches a plateau at $\phi_b \geq 0.45\,\%$ (Torres Maldonado *et al.* 2022). We assessed the impacts of advection and diffusion by quantifying the Péclet (Pe) number. Within the linear regime ($\phi_b < 0.45\,\%$), we noticed a decrease in advection effects due to particle hindrance, accompanied by an increase in diffusion effects owing to increased particle fluctuations. In the vicinity of the plateau regime, both settling (advection) and random motion (diffusion) exhibit near-equivalence ($Pe \approx 1$). The emergence of this plateau regime can be explained by (3.2), quantifying Γ, and (3.5), determining Γ_{cr}. Interestingly, our results manifest a crossover at $\phi_b \approx 0.45\,\%$ between the experimental Rayleigh number and the estimated critical Rayleigh number (figure 4). This suggests that under $\phi_b < 0.45\,\%$, bacteria engage in random swimming, with minimal oxygen-related effects in the upper portion of the container. However, at $\phi_b \geq 0.45\,\%$, oxygen plays a prominent role, giving rise to intricate bioconvection patterns, as depicted in figure 5. In both these regimes, the input of energy via bacterial swimming motions significantly influences the sedimentation process, thereby enhancing particle diffusivities.

4. Conclusion

We experimentally investigated the sedimentation dynamics of colloidal particles within dilute suspensions of swimming bacteria. Our overall observation reveals that bacterial activity enhances the effective diffusivities (D_{eff}) and the correlation length L_u of colloidal particles. Moreover, our experimental analysis of spherical particle behaviour exhibits two distinct regimes. The first regime showcases a linear increase in both D_{eff}

and L_u in correlation with bacterial concentration (ϕ_b) up to $\phi_b < 0.45\,\%$. In contrast, once $\phi_b \geq 0.45\,\%$, both D_{eff} and L_u remain unchanged despite varying the bacterial concentration. To uncover the foundation of these distinct regimes, we calculated the experimental Rayleigh number (Γ) and the critical Rayleigh number (Γ_{cr}), respectively, using experimentally measured quantities. Solving for these non-dimensional quantities reveals a transition point in bacterial concentration that divides the two observed regimes within our experiments. This transition suggests that the system becomes unstable beyond $\phi_b \geq 0.45\,\%$, leading to complex bioconvection patterns. This inference gains further validation through a separate set of experiments using dye as a tracer within the fluid. For $\phi_b < 0.45\,\%$, the variance demonstrates diffusive behaviour. Interestingly, when $\phi_b \geq 0.45\,\%$, the variance initially exhibits diffusive behaviour for short times, followed by a transition to convection-like behaviour.

In summary, our findings show that the reduction in convective transport of colloidal particles is attributed to the increased bacterial-driven convective motion driven by oxygen gradients. This suggests that the experimental boundary conditions could be modified by using oxygen-permeable materials to control the bioconvection phenomenon. Future work involving diverse colloidal sizes and swimmer actuation modes (such as pusher versus puller) holds the potential to elucidate whether the insights obtained from our particle–bacteria interaction study can be generalized to others.

Acknowledgements. The authors thank D. Durian and S. Spagnolie for fruitful discussions.

Funding. This work was partially supported by the National Science Foundation (NSF) DMR-1709763.

Declaration of interests. The authors report no conflict of interest.

Author ORCIDs.
Bryan O. Torres Maldonado https://orcid.org/0000-0002-0520-1907;
Shravan Pradeep https://orcid.org/0000-0001-7483-2385;
Ranjiangshang Ran https://orcid.org/0000-0001-5810-1312;
Douglas Jerolmack https://orcid.org/0000-0003-4358-6999;
Paulo E. Arratia https://orcid.org/0000-0002-2566-2663.

References

Adler, M., Erickstad, M., Gutierrez, E. & Groisman, A. 2012 Studies of bacterial aerotaxis in a microfluidic device. *Lab on a Chip* **12**, 4835–4847.

Arrieta, J., Polin, M., Saleta-Piersanti, R. & Tuval, I. 2019 Light control of localized photobioconvection. *Phys. Rev. Lett.* **123**, 158101.

Baracchini, O. & Sherris, J.C. 1959 The chemotactic effect of oxygen on bacteria. *J. Pathol. Bacteriol.* **77** (2), 565–574.

Bees, M.A. 2020 Advances in bioconvection. *Annu. Rev. Fluid Mech.* **52** (1), 449–476.

Bouvard, J., Douarche, C., Mergaert, P., Auradou, H. & Moisy, F. 2022 Direct measurement of the aerotactic response in a bacterial suspension. *Phys. Rev.* E **106**, 034404.

Bouvard, J., Moisy, F. & Auradou, H. 2023 Ostwald-like ripening in the two-dimensional clustering of passive particles induced by swimming bacteria. *Phys. Rev.* E **107** (4), 044607.

Brosseau, Q., Ran, R., Graham, I., Jerolmack, D.J. & Arratia, P.E. 2022 Flow and aerosol dispersion from wind musical instruments. *Phys. Fluids* **34** (8), 087115.

Carpenter, J.H. 1966 New measurements of oxygen solubility in pure and natural water. *Limnol. Oceanogr.* **11**, 264–277.

Chen, D.T.N., Lau, A.W.C., Hough, L.A., Islam, M.F., Goulian, M., Lubensky, T.C. & Yodh, A.G. 2007 Fluctuations and rheology in active bacterial suspensions. *Phys. Rev. Lett.* **99**, 148302.

Crocker, J.C. & Grier, D.G. 1996 Methods of digital video microscopy for colloidal studies. *J. Colloid Interface Sci.* **179** (1), 298–310.

DABELOW, L., BO, S. & EICHHORN, R. 2019 Irreversibility in active matter systems: fluctuation theorem and mutual information. *Phys. Rev.* X **9** (2), 021009.

EINSTEIN, A. 1905 On the movement of small particles suspended in a stationary liquid demanded by the molecular-kinetic theory of heat. *Ann. Phys.* **17** (854), 549–560.

FALKOWSKI, P. 2012 The power of plankton. *Nature* **483**, S17–S20.

FALKOWSKI, P.G., BARBER, R.T. & SMETACEK, V. 1998 Biogeochemical controls and feedbacks on ocean primary production. *Science* **281** (5374), 200–206.

GACHELIN, J., MIÑO, G., BERTHET, H., LINDNER, A., ROUSSELET, A. & CLÉMENT, E. 2013 Non-Newtonian viscosity of *Escherichia coli* suspensions. *Phys. Rev. Lett.* **110** (26), 268103.

GINOT, F., SOLON, A., KAFRI, Y., YBERT, C., TAILLEUR, J. & COTTIN-BIZONNE, C. 2018 Sedimentation of self-propelled Janus colloids: polarization and pressure. *New J. Phys.* **20** (11), 115001.

GINOT, F., THEURKAUFF, I., LEVIS, D., YBERT, C., BOCQUET, L., BERTHIER, L. & COTTIN-BIZONNE, C. 2015 Nonequilibrium equation of state in suspensions of active colloids. *Phys. Rev.* X **5** (1), 011004.

HAN, P. & BARTELS, D.M. 1996 Temperature dependence of oxygen diffusion in H_2O and D_2O. *J. Phys. Chem.* **100** (13), 5597–5602.

HERNDL, G.J. & REINTHALER, T. 2013 Microbial control of the dark end of the biological pump. *Nat. Geosci.* **6** (9), 718–724.

HILL, N.A. & PEDLEY, T.J. 2005 Bioconvection. *Fluid Dyn. Res.* **37** (1–2), 1.

HILL, N.A., PEDLEY, T.J. & KESSLER, J.O. 1989 Growth of bioconvection patterns in a suspension of gyrotactic micro-organisms in a layer of finite depth. *J. Fluid Mech.* **208**, 509–543.

HILLESDON, A.J. & PEDLEY, T.J. 1996 Bioconvection in suspensions of oxytactic bacteria: linear theory. *J. Fluid Mech.* **324**, 223–259.

HILLESDON, A.J., PEDLEY, T.J. & KESSLER, J.O. 1995 The development of concentration gradients in a suspension of chemotactic bacteria. *Bull. Math. Biol.* **57** (2), 299–344.

HONDA, R., MATSUURA, N., SORN, S., ASAKURA, S., MORINAGA, Y., VAN HUY, T., SABAR, M.A., MASAKKE, Y., HARA-YAMAMURA, H. & WATANABE, T. 2023 Transition of antimicrobial resistome in wastewater treatment plants: impact of process configuration, geographical location and season. *NPJ Clean Water* **6** (1), 46.

JÁNOSI, I.M., KESSLER, J.O. & HORVÁTH, V.K. 1998 Onset of bioconvection in suspensions of *Bacillus subtilis*. *Phys. Rev.* E **58**, 4793–4800.

JEANNERET, R., PUSHKIN, D.O., KANTSLER, V. & POLIN, M. 2016 Entrainment dominates the interaction of microalgae with micron-sized objects. *Nat. Commun.* **7**, 12518.

JEPSON, A., MARTINEZ, V.A., SCHWARZ-LINEK, J., MOROZOV, A. & POON, W.C.K. 2013 Enhanced diffusion of nonswimmers in a three-dimensional bath of motile bacteria. *Phys. Rev.* E **88** (4), 041002.

KASYAP, T.V., KOCH, D.L. & WU, M. 2014 Hydrodynamic tracer diffusion in suspensions of swimming bacteria. *Phys. Fluids* **26** (8), 081901.

KIM, M.J. & BREUER, K.S. 2004 Enhanced diffusion due to motile bacteria. *Phys. Fluids* **16** (9), L78–L81.

KURTULDU, H., GUASTO, J.S., JOHNSON, K.A. & GOLLUB, J.P. 2011 Enhancement of biomixing by swimming algal cells in two-dimensional films. *Proc. Natl Acad. Sci.* **108** (26), 10391–10395.

LEPTOS, K.C., GUASTO, J.S., GOLLUB, J.P., PESCI, A.I. & GOLDSTEIN, R.E. 2009 Dynamics of enhanced tracer diffusion in suspensions of swimming eukaryotic microorganisms. *Phys. Rev. Lett.* **103** (19), 198103.

LI, J., RAN, R., WANG, H., WANG, Y., CHEN, Y., NIU, S., ARRATIA, P.E. & YANG, S. 2021 Aerodynamics-assisted, efficient and scalable kirigami fog collectors. *Nat. Commun.* **12** (1), 5484.

VAN LOOSDRECHT, M.C.M. & BRDJANOVIC, D. 2014 Anticipating the next century of wastewater treatment. *Science* **344** (6191), 1452–1453.

LÓPEZ, H.M., GACHELIN, J., DOUARCHE, C., AURADOU, H. & CLÉMENT, E. 2015 Turning bacteria suspensions into superfluids. *Phys. Rev. Lett.* **115** (2), 028301.

LORENZO, J.M., MUNEKATA, P.E., DOMINGUEZ, R., PATEIRO, M., SARAIVA, J.A. & FRANCO, D. 2018 Chapter 3 - main groups of microorganisms of relevance for food safety and stability: general aspects and overall description. In *Innovative Technologies for Food Preservation* (ed. F.J. Barba, A.S. Sant'Ana, V. Orlien & M. Koubaa), pp. 53–107. Academic Press.

MAGGI, C., LEPORE, A., SOLARI, J., RIZZO, A. & DI LEONARDO, R. 2013 Motility fractionation of bacteria by centrifugation. *Soft Matt.* **9** (45), 10885–10890.

MARCHETTI, M.C., JOANNY, J.F., RAMASWAMY, S., LIVERPOOL, T.B., PROST, J., RAO, M. & SIMHA, R.A. 2013 Hydrodynamics of soft active matter. *Rev. Mod. Phys.* **85**, 1143–1189.

MARTÍNEZ-SALAS, E., MARTÍN, J.A. & VICENTE, M. 1981 Relationship of *Escherichia coli* density to growth rate and cell age. *J. Bacteriol.* **147** (1), 97–100.

MIÑO, G., MALLOUK, T.E., DARNIGE, T., HOYOS, M., DAUCHET, J., DUNSTAN, J., SOTO, R., WANG, Y., ROUSSELET, A. & CLEMENT, E. 2011 Enhanced diffusion due to active swimmers at a solid surface. *Phys. Rev. Lett.* **106** (4), 048102.

MORAN, J.L. & POSNER, J.D. 2017 Phoretic self-propulsion. *Annu. Rev. Fluid Mech.* **49** (1), 511–540.
NASH, R.W., ADHIKARI, R., TAILLEUR, J. & CATES, M.E. 2010 Run-and-tumble particles with hydrodynamics: sedimentation, trapping, and upstream swimming. *Phys. Rev. Lett.* **104** (25), 258101.
NEALSON, K.H. 1997 Sediment bacteria: who's there, what are they doing, and what's new? *Annu. Rev. Earth Planet. Sci.* **25** (1), 403–434.
PALACCI, J., COTTIN-BIZONNE, C., YBERT, C. & BOCQUET, L. 2010 Sedimentation and effective temperature of active colloidal suspensions. *Phys. Rev. Lett.* **105** (8), 088304.
PATTESON, A.E., GOPINATH, A. & ARRATIA, P.E. 2016*a* Active colloids in complex fluids. *Curr. Opin. Colloid Interface Sci.* **21**, 86–96.
PATTESON, A.E., GOPINATH, A., GOULIAN, M. & ARRATIA, P.E. 2015 Running and tumbling with *E. coli* in polymeric solutions. *Sci. Rep.* **5**, 15761.
PATTESON, A.E., GOPINATH, A., PUROHIT, P.K. & ARRATIA, P.E. 2016*b* Particle diffusion in active fluids is non-monotonic in size. *Soft Matt.* **12** (8), 2365–2372.
PEDLEY, T.J. & KESSLER, J.O. 1992 Hydrodynamic phenomena in suspensions of swimming microorganisms. *Annu. Rev. Fluid Mech.* **24** (1), 313–358.
PRADEEP, S. & ARRATIA, P.E. 2022 Bacteria: to biofilm or not to biofilm. *eLife* **11**, e80891.
RAFAÏ, S., JIBUTI, L. & PEYLA, P. 2010 Effective viscosity of microswimmer suspensions. *Phys. Rev. Lett.* **104** (9), 098102.
RAMASWAMY, S. 2010 The mechanics and statistics of active matter. *Annu. Rev. Condens. Matt. Phys.* **1** (1), 323–345.
RAN, R., BROSSEAU, Q., BLACKWELL, B.C., QIN, B., WINTER, R.L. & ARRATIA, P.E. 2021 Bacteria hinder large-scale transport and enhance small-scale mixing in time-periodic flows. *Proc. Natl Acad. Sci. USA* **118** (40), e2108548118.
RAN, R., GAGNON, D.A., MOROZOV, A. & ARRATIA, P.E. 2022 Polymers in swarming bacterial turbulence. Preprint, arXiv:2111.00068v2.
ROBERTO, A.A., VAN GRAY, J.B. & LEFF, L.G. 2018 Sediment bacteria in an urban stream: spatiotemporal patterns in community composition. *Water Res.* **134**, 353–369.
RUSSEL, W.B., RUSSEL, W.B., SAVILLE, D.A & SCHOWALTER, W.R. 1991 *Colloidal Dispersions*. Cambridge University Press.
SAVAGE, N. 2011 Algae: the scum solution. *Nature* **474** (7352), S15–S16.
SCHALLENBERG, M. & KALFF, J. 1993 The ecology of sediment bacteria in lakes and comparisons with other aquatic ecosystems. *Ecology* **74** (3), 919–934.
SCHWARZ-LINEK, J., ARLT, J., JEPSON, A., DAWSON, A., VISSERS, T., MIROLI, D., PILIZOTA, T., MARTINEZ, V.A. & POON, W.C.K. 2016 *Escherichia coli* as a model active colloid: a practical introduction. *Coll. Surf.* B*: Biointerfaces* **137**, 2–16.
SEGRÈ, P.N., HERBOLZHEIMER, E. & CHAIKIN, P.M. 1997 Long-range correlations in sedimentation. *Phys. Rev. Lett.* **79**, 2574–2577.
SINGH, J., PATTESON, A., TORRES MALDONADO, B., PUROHIT, P.K. & ARRATIA, P.E. 2021 Bacteria hinders particle sedimentation. *Soft Matt.* **17**, 4151–4160.
SUN, X., PEENI, B.A., YANG, W., BECERRIL, H.A. & WOOLLEY, A.T. 2007 Rapid prototyping of poly(methyl methacrylate) microfluidic systems using solvent imprinting and bonding. *J. Chromatogr.* A **1162** (2), 162–166.
SWARTZ, J.R. 2001 Advances in *Escherichia coli* production of therapeutic proteins. *Curr. Opin. Biotechnol.* **12** (2), 195–201.
TAILLEUR, J. & CATES, M.E. 2008 Statistical mechanics of interacting run-and-tumble bacteria. *Phys. Rev. Lett.* **100** (21), 218103.
TEE, S.-Y., MUCHA, P.J., CIPELLETTI, L., MANLEY, S., BRENNER, M.P., SEGRE, P.N. & WEITZ, D.A. 2002 Nonuniversal velocity fluctuations of sedimenting particles. *Phys. Rev. Lett.* **89**, 054501.
THIFFEAULT, J.-L. & CHILDRESS, S. 2010 Stirring by swimming bodies. *Phys. Lett.* A **374** (34), 3487–3490.
TORRES MALDONADO, B.O., RAN, R., GALLOWAY, K.L., BROSSEAU, Q., PRADEEP, S. & ARRATIA, P.E. 2022 Phase separation during sedimentation of dilute bacterial suspensions. *Phys. Fluids* **34** (11), 113305.
VACHIER, J. & MAZZA, M.G. 2019 Dynamics of sedimenting active Brownian particles. *Eur. Phys. J.* E **42** (1), 11.
VERMEULEN, N., KEELER, W.J., NANDAKUMAR, K. & LEUNG, K.T. 2008 The bactericidal effect of ultraviolet and visible light on *Escherichia coli*. *Biotechnol. Bioengng* **99** (3), 550–556.
WAGER, H.W.T. 1911 VII. On the effect of gravity upon the movements and aggregation of *Euglena viridis*, Ehrb., and other micro-organisms. *Phil. Trans. R. Soc. Lond. Ser.* B *Contain. Pap. Biol. Character* **201** (274–281), 333–390.

WANG, Z., CHEN, H.Y., SHENG, Y.J. & TSAO, H.K. 2014 Diffusion, sedimentation equilibrium, and harmonic trapping of run-and-tumble nanoswimmers. *Soft Matt.* **10** (18), 3209–3217.

WU, X.-L. & LIBCHABER, A. 2000 Particle diffusion in a quasi-two-dimensional bacterial bath. *Phys. Rev. Lett.* **84** (13), 3017–3020.

ZHANG, L., TU, D., LI, X., LU, W. & LI, J. 2020 Impact of long-term industrial contamination on the bacterial communities in urban river sediments. *BMC Microbiol.* **20** (1), 254.